Desalination and Water Treatment
www.deswater.com

doi: 10.5004/dwt.2021.26844

219 (2021) 232–239
April

Berthing force of windsurfing under accompanying wave action of wave group

Rongjun Zhu

Sports Teaching and Research Department, Jiangsu Police Institute, Lianyungang 210031, China, email: luanxuejing@163.com

Received 15 August 2020; Accepted 23 November 2020

ABSTRACT

In order to ensure the safety of windsurfing and study the steady-state of sheltered water area, a method to study the berthing force of windsurfing under the accompanying wave action of wave group was put forward. The accompanying wave action of the wave group was analyzed. Then, the smooth particle hydrodynamics method was used to build a mathematical model for simulating the interaction between the non-linear wave and the combination structure of sailboard. The relationship between the accompanying wave action of the wave group and the berthing force of windsurfing was verified by the mathematical model. Meanwhile, the forming condition of the berthing force of windsurfing was simulated in the water flume of the laboratory. Finally, the berthing force of windsurfing was studied. Simulation results show that when the angle between the sail and the horizontal plane is about 130°, the proposed method has strong adaptability and effectiveness, so it can effectively ensure the safety of windsurfing.

Keywords: Accompanying wave action of wave group; Windsurfing; Berthing force; Non-linear wave

1. Introduction

Wave is a very common natural phenomenon in a huge water area [1,2]. The ripples and small waves on rivers and lakes and the huge waves and tsunamis on sea surface belong to the category of waves. The wave will influence the navigation of ships and damaged buildings along the sea, rivers and lakes. The damage mainly includes two forms: one is a long-term effect. For example, the scouring intensity of the wave is not large in a short time, but the long-term effect eventually leads to the damage of embankment, especially the damage to the soil or the loose embankment. The other is the sudden effect. For example, the short-term huge waves, the low-frequency tsunami will wash the embankment in a short time. It is often more serious than in the first situation.

In the field of engineering, the damage of wave to embankment structure has always been a hot topic [3]. The structure of the sloping bank is the most traditional and most extensive form in the shoreline structure, which can be used in breakwater, wharf, coastal protection, slope protection, earth dam of reservoir, wave resistance project. In port design and embankment engineering, the study of berthing force is always an important link. As one of the main loads of environmental dynamics, the wave also plays an important role in windsurfing. Some scholars have studied the berthing force of sailboard under the action of random waves. For example, Huang et al. [4] proposed the empirical formula of the wave envelope spectrum based on the measured data and established the numerical and physical simulation methods of the wave group. After the dimensionless, Ding et al. [5] got the empirical formula of wave envelope spectrum which was more suitable for wind and waves and put forward reasonable principle to select parameter value. Wu et al. [9] carried out the numerical simulation of multi-directional irregular wave group

propagation based on the numerical simulation of one-way wave group and wave train and analyzed the propagation process of multi-directional irregular wave group.

Although some significant results have been achieved by the above methods, they hadn't considered terrible sea conditions and ignored a stable state. Therefore, the research on the berthing force of windsurfing under the accompanying wave action of wave group was designed and proposed. Through the simulation experimental data, the comprehensive effectiveness of the proposed method is fully verified.

2. Methods

2.1. Analysis of accompanying wave action of the wave group

From the mid-19th century to the early 20th century, many scientists put forward some wave theories to describe the sea wave. These theories can be divided into two fields. The first field is to study the motion of a single particle in the liquid from the perspective of hydrodynamics, including linear wave theory and non-linear wave theory. Linear wave theory mainly refers to the micro amplitude wave theory (Airy wave theory). According to different characteristics of a wave, non-linear wave theory includes limited amplitude wave theory (Stokes wave theory), Solitary wave theory and Conidial wave theory. In the other field, the wave is regarded as a random process. Its randomness is studied to reveal the distribution characteristic of wave energy in the wave and describe the motion state of a particle in a statistical sense. The motion form of the sailboard is shown in Fig. 1.

For the joint action of wave and current, the current method is the regular linear wave. Generally, the movement laws of water particles under the separate action of wave and current are superposed to get the total law of joint action of wave and current. For regular non-linear wave or irregular wave (random wave), this kind of superposition often brings big error. The more effective method is a regular non-linear wave. It is described by the high-order wave theory based on stream function or calculated by the direct numerical analysis of non-linear waves. The irregular wave is described by the statistical analysis of random process and wave spectrum.

All kinds of regular wave theories must be based on a basic assumption that wave elements (wave height, wavelength and wave period) are fixed in the process of wave propagation. The wave theory [4–6] digressed from this assumption is called irregular wave theory. Regular wave theory includes linear wave theory and non-linear wave theory.

Before introducing the linear wave theory, it is necessary to introduce several important wave parameters first. H denotes the elevation (the vertical distance from wave crest to wave trough). L denotes the wavelength. d denotes the water depth. H/d denotes the relative wave height. d/L denotes the relative water depth. U_R denotes the relative wavelength. L/d denotes Urse11 number. Based on linear wave theory and micro amplitude wave theory (Airy wave theory), the velocity potential function $\phi(x,z,t)$ of fluid is used to research the wave motion. The theoretical assumption is that the velocity of the water particle of the wave is slow, and its fluctuation range is very small. The bottom of the water body is a horizontal impermeable level. The basic equation is:

$$\frac{p}{\rho} + gz + \frac{1}{2}\left(u^2 + v^2\right) + \frac{\partial\phi}{t} = 0 \tag{1}$$

In the formula, p represents the pressure at different points in the fluid; u denotes the horizontal velocity of water particles at each point in the flow field and v denotes vertical velocity [7,8]. According to the definition of velocity potential, we can find that:

$$u = \frac{\partial\phi}{x} \tag{2}$$

$$v = \frac{\phi}{\partial z} \tag{3}$$

The boundary conditions of the potential flow field are shown as follows:

- On the bottom of the sea $z = -d$, $v = \frac{\phi}{\partial z} = 0$;
- At the water surface $z = \eta_0$, there are two boundary conditions.

The dynamic boundary conditions of free water surface are:

$$g\eta_0 + \frac{1}{2}\left(u^2 + v^2\right) + \frac{\partial\phi}{t} = 0 \tag{4}$$

The motion boundary conditions of free water surface are:

$$\frac{\partial\phi}{z}|_{s-\eta_0} = \frac{\eta_0}{\partial z} + \frac{\eta_0}{\partial x}\cdot\frac{\partial\phi}{x}|_{s-\eta_0} \tag{5}$$

According to the setting of "slow-wave speed and small wave amplitude", the non-linear $\frac{1}{2}$ $(u^2 + v^2)$ and $\frac{\eta_0}{\partial x}\cdot\frac{\partial\phi}{x}$ in Eqs. (3) and (4) can be ignored. The dynamic condition and motion boundary condition can be transformed into linear problems [9]. After solving the basic equation, we can get:

Fig. 1. Windsurfing.

- Potential function in finite water depth:

$$\phi = \frac{gH}{2\omega} \cdot \frac{k(d+z)}{kd} \sin(kx - \omega t) \tag{6}$$

In Eq. (6), ω represents the circular frequency of the wave, and k represents the wavenumber.

$$k = \frac{2\pi}{L} \tag{7}$$

- Potential function in infinite water depth [10,11]:

$$U_R = \frac{gH}{2\omega} e^{kz} \sin(kx - \omega t) \tag{8}$$

Compared with the linear wave theory, the non-linear wave theory has similar basic equations and three boundary conditions about potential function $\phi(x,y,z)$. However, the non-linear wave theory extends the non-linear term in boundary condition by higher-order non-linear term or series and then performs a numerical analysis on the solution of basic equation [12]. Finally, the motion equation of a water particle that can meet the more complex wave can be obtained.

When U_R increases gradually, the non-linear second-order term in U_R will gradually occupy a large proportion. Even if the relative wave height H/d is small, the linear wave theory is no longer applicable. It is necessary to consider the use of non-linear wave theory.

When U_R < 10 and the relative depth d/L of water is within the limited depth, Stoke's high-order wave theory can be adopted. this theory is generally suitable for the case of deep water and large wave steepness. When the relative wave height H/d is close to and less than 1, the relative depth is within shallow water, that is d/L < 1/8~1/10, Stoke's theory is no longer applicable. The theory of conoidal waves can be adopted [13]. When the water depth continues to decrease or the relative wavelength continues to increase to $\frac{L}{d} \to \infty$, the theory of conoidal wave approaches to the theory of solitary wave.

The theory of regular wave is based on the randomness of large-scale wave motion on the sea. The wave elements change with different water particles and a different time, without any repeatability.

Because the wave is formed by wind, and the wind field near the sea surface is complex. The wind speed and wind direction are changeable. The wave surface also has a reacting force to the wind field. In addition, the internal turbulence of wave and wave surface-breaking make the sea wave become a highly irregular and non-repetitive physical phenomenon. In fact, it is an irregular wave (random wave). The combination of wave spectrum analysis in random process and statistical analysis of the data system is an important way to study random waves.

In actual engineering, the study of waves by irregular wave (or random wave) [14,15] can correctly describe the sea wave and design the sailboard more safely and reasonably.

When waves move from deep water area to shallow water area, the change of water depth will cause the change of wave elements. For regular linear waves, we mainly study the change of wave elements through "wave energy flow".

Wave energy flow refers to the average value of wave power in a wave period. It is equal to the average value in a wave period of the sum of the force exerted by the wave with the length of single-width peak line on the point on a vertical plane parallel to wave peak line and the velocity product of water particles of a wave passing through the corresponding point on the vertical plane [16]. Based on the linear micro amplitude wave theory and limited water depth, the wave energy flow can be calculated by Eq. (9) without considering the influence of free wave surface on the boundary of potential flow field:

$$\text{FLUX} = \begin{cases} \frac{E_W}{T} \cdot \frac{1}{2}\left(1 + \frac{2k \cdot d}{2k \cdot h \cdot d}\right) \\ \frac{E_W \cdot n}{T} \end{cases} \tag{9}$$

In Eq. (9), FLUX denotes the wave energy flow. k denotes the wavenumber. E_W denotes the wave energy. n denotes the transmission rate of wave energy, which mainly refers to the ratio of the energy transmitted by fluctuation to total energy stored in a wave, then:

$$n = \frac{1}{2} \cdot \left(1 + \frac{2k \cdot d}{2k \cdot h \cdot d}\right) \tag{10}$$

Based on the motion equation of water particle after regular wave breaking on the slope, the distribution of wave velocity and wave pressure in the process of motion of sailboard is derived semi-theoretically and semi-empirically [17,18]. It is assumed that the slope is uniform and smooth, and the wave is incident vertically and positively. The horizontal lateral force formed by the breaking wave on the slope can be ignored.

The critical water depth of the wave on the slope is d_0. The elevation of wave crest A higher than the static water level is H_0. After the wave is crushed, the water particle of the wave crest lashes the slope in the form of jet-flow according to the parabola. The maximum wave pressure and the maximum velocity are generated at the intersection B of a jet-flow and steep slope.

In order to describe the motion of the sailboard, two coordinate systems are established [19]: fixed coordinate system O–xyz and dynamic coordinate system O'–$x'y'z'$. The original points of coordinate systems are located at the center of gravity of the sailboard. The two coordinate systems coincide in the initial state. The linear displacement of the sailboard is the movement with the sailboard coordinate system O'–$x'y'z'$ relative to the fixed coordinate system O–xyz. It is defined as:

$$\Delta = (\Delta X, \Delta Y, \Delta Z) \tag{11}$$

The angle displacement of the sailboard is the rotation angle of the axis xyz of coordinate [20,21]. It is set as:

$$\theta = \left(\theta_x, \theta_y, \theta_z\right) \tag{12}$$

The coordinates of point *B* is:

$$Y_B = \frac{X_B}{m'} \tag{13}$$

The temporal course of the first-order wave force is obtained by convoluting the impulse response function of wave force in the time domain with the wave surface.

$$F_i\left(t\right) = \int_0^t h_i\left(t-\tau\right)\eta_1 d\tau \tag{14}$$

$$h_i\left(t\right) = \mathrm{Re}\left[\frac{1}{\pi}\int_0^\infty H_i\left(\omega\right)e^{i\omega t}d\omega\right] \tag{15}$$

where $H_i(\omega)$ represents the first-order wave excitation force of the object under the action of the regular wave with unit amplitude. $h_i(\omega)$ represents the first-order pulse response function in the time domain. $F_i(t)$ represents the wave force in the first-order time domain. η_1 represents the wave surface of the wave group. The second-order wave force is an important external environmental force for the ship to do low-frequency motion. It can be divided into differential frequency force and sum-frequency force. The differential frequency force will cause the low-frequency slow drift motion of the ship. The far-field method is used to calculate the average drift force in regular waves, and the average drift force is used to approximate the difference frequency force to meet the engineering. The Newman assumption is adopted to process the second-order wave force with low frequency.

$$F^{(2)}\left(t\right) = \sum_{i=1}^{N}\sum_{j=1}^{N}\xi_i\xi_j P_{ii}\cos\left[\left(\omega_i-\omega_j\right)t+\left(\varepsilon_i+\varepsilon_j\right)\right] \tag{16}$$

2.2. Study on berthing force of windsurfing under the accompanying wave action of the wave group

The smooth particle hydrodynamics (SPH) method is a numerical discretization method [22,23], which discretizes arbitrary functions and their spatial derivatives into a series of interactions between particles with independent mass and volume through integral approximation and particle approximation. The integral approximation is the expression of the "smooth" concept in SPH. The particle approximation is the expression of the "particle" concept in SPH.

- *Integral approximation*:

The field function at the target point in space can be written as the following integral form:

$$f\left(x_0\right) = f_\Omega f\left(x\right)\delta\left(x_0-x\right)dx \tag{17}$$

In Eq. (17), x_0 is the position of the target point. Ω is the principal domain of the integral domain. δ is the Dirac δ function.

In the SPH method, the kernel function is introduced to approximate the substitution function, and the approximate integral form of the field function is obtained.

In the SPH method, the kernel function $W(x_0,-x,h)$ is introduced to approximate substitute for δ function, and then the approximate integral form of field function is obtained.

$$\left\langle f\left(x_0\right)\right\rangle = f_\Omega f\left(x\right)W\left(x_0,-x,h\right)dx \tag{18}$$

In the formula, *h* denotes the smoothing length, which is related to the physical problem. In the numerical calculation, the smoothing length is 1.5 times more than the initial particle spacing of the model.

According to Eq. (17), the integral approximate expression of the spatial derivative of the field function can be obtained [24].

$$\left\langle \nabla\cdot f\left(x_0\right)\right\rangle = f_\Omega\left[\nabla\cdot f\left(x\right)\right]W\left(x_0,-x,h\right)dx \tag{19}$$

After Gaussian transformation and arranging the Eq. (19), we can get:

$$\left\langle \nabla\cdot f\left(x_0\right)\right\rangle = -f_\Omega f\left(x\right)\cdot\nabla W\left(x_0,-x,h\right)dx \tag{20}$$

In the numerical calculation, the quintic kernel function is adopted, and its mathematical formula is written as follows:

$$W\left(x_0,-x,\kappa h\right) = a_d\begin{cases}\left(1-\dfrac{q}{2}\right)^4\left(2q+1\right), 0\le q<2\\ 0, q\ge 2\end{cases} \tag{21}$$

- *Particle approximation*:

The target particle *i* is located at the center of the integral domain, and a series of particles *j* with independent mass and volume are distributed around it. The radius of the support region of particle *i* is κ*h*. Only the interaction between the particle *i* and the particle *j* whose linear distance is less than κ*h* needs to be considered. In this way, the integral approximate expression in Eq. (18) of field function can be discretized into:

$$\left\langle f\left(x_i\right)\right\rangle = \begin{cases}f_\Omega f\left(x\right)W\left(x_i,-x,\kappa h\right)\\ \displaystyle\sum_{j=1}^{N} f\left(x_j\right)W_{ij}\Delta V_j\end{cases} \tag{22}$$

Because $m_j = \Delta V_j\rho_j$, the Eq. (22) can also be written:

$$\left\langle \nabla\cdot f\left(x_i\right)\right\rangle = \sum_{j=1}^{N}\frac{m_j}{\rho_j}f\left(x_j\right)\nabla_i W_{ij} \tag{23}$$

In the formula:

$$\nabla_i W_{ij} = \frac{x_i-x_j}{r_{ij}}\frac{\partial W_{ij}}{\partial r_{ij}} \tag{24}$$

In Eq. (24), r_{ij} represents the distance between particle i and particle j.

The motion of a viscous fluid can be described by the continuity equation and the NS equation. In the Lagrangian system it can be written in the following form:

$$\frac{d\rho}{dt} = -\rho\nabla \cdot v \tag{25}$$

$$\frac{dv}{dt} = -\frac{1}{\rho}\nabla p + v\nabla^2 v + g \tag{26}$$

In the formula,

$$\nabla = \left(\frac{\partial}{\partial x}, \frac{\partial}{\partial y}, \frac{\partial}{\partial z}\right) \tag{27}$$

The motion position of the fluid is calculated by Eq. (27):

$$\frac{dv}{dt} = v \tag{28}$$

When the SPH method is used to discretize the fluid continuity Eq. (24), the continuity equation is rewritten as follows:

$$\frac{d\rho}{dt} = -\nabla \cdot \left(\rho v\right) + v \cdot \nabla\rho \tag{29}$$

The above analysis shows that the density of fluid particles is determined by the relative velocity and relative position between particles. Due to the randomness of particle distribution and the limited number of target particles in the support domain, it is impossible to compensate for the randomness of position distribution by increasing the number of particles, so the impact of other particles in the support domain on the target particles is also random, resulting in the weak fluctuation of particle density. Smoothing the density of particles in the calculation domain can effectively alleviate the non-physical oscillation of the density field [25]. Therefore, the zero-order Shepard density filtering method is adopted. The specific method is that the density of fluid particles modified as follows:

$$\rho_i = \sum_{j=1}^{N} m_j \bar{W}_{ij} \tag{30}$$

In Eq. (30), $\bar{W}_{ij}$ represents the modified kernel function, and the specific calculation can be expressed as follows:

$$\bar{W}_{ij} = \frac{W_{ij}}{\sum_{j=1}^{N} \frac{\rho_j}{m_j} W_{ij}} \tag{31}$$

When the SPH method is used to discretize the momentum Eq. (25), the viscosity of a fluid is not considered at first. The momentum equation is rewritten as follows:

$$\frac{dv}{dt} = -\nabla\left(\frac{p}{\rho}\right) - \frac{p}{\rho^2}\nabla\rho + g \tag{32}$$

The traditional kinetics boundary particle method in the SPH model is improved. The stability of the fluid pressure field near the solid wall boundary is enhanced without sacrificing the convenience of the kinetics boundary particle method so that the calculation accuracy of fluid force on the solid wall boundary is improved [26]. The density on the boundary and the average density of fluid particles are calculated by the continuity equation. The specific mathematical expression is shown as follows.

$$\rho_i^t = \chi\rho_i + \left(1-\chi\right)\bar{\rho}_j \tag{33}$$

When calculating the average density of the fluid particles, the influence of the gradient of the fluid density field should be eliminated at first.

$$\bar{\rho}_j = \frac{1}{N}\sum_{j=1}^{N}\left(\rho_j - \nabla\rho_j \cdot x_{ij}\right) \tag{34}$$

The following forms can be obtained through the state equation.

$$\nabla\rho_j = \frac{1}{c_0^2}\left(\frac{\rho_j}{\rho_0}\right)^{(1-\gamma)} \Delta p_j \tag{35}$$

Generally, the radius of the support region of particles in the SPH model is within 2–3 times particle spacing. The kernel function W_{ij} decreases rapidly with the increase of particle spacing, and the fluid particles closest to DBPs in correlative formulas can play a role in density smoothness, so the density averaging effect of kernel function is not as good as the direct averaging density of fluid-particle [27].

Based on the above analysis, the relationship between the berthing force and accompanying wave action of the wave group can be analyzed by the mathematical model.

3. Simulation experiment

In order to verify the comprehensive effectiveness of the proposed method, a simulation experiment was carried out. The physical model test of the interaction between the windsurfing and wave under different accompanying wave action of wave group was carried out in the wave flume of the laboratory.

The windsurfing is obtained by image measurement and data processing technology. The physical model tests the motion response of a sailboard under the action of waves. The specific experimental results are shown as follows:

- Firstly, the test of free damping roll motion of sailboard was carried out. On the premise of keeping the center of mass of the sailboard unchanged, a vertical downward load was applied to the corner of the sailboard to tilt the sailboard [28]. The angle between the sailboard and the horizontal plane was about 130°. When the experiment began, the load was released instantly. The sailboard freely damps and rolls around the center of mass. During the rolling motion, the movement of the center of mass of the sailboard is relatively small, so it can be ignored [29–31].

The experiment of the interaction between waves and windsurfing was carried out. In this experiment, multiple groups of different wave conditions and wave elements were selected. The specific results are shown in Table 1.

Based on the above wave elements, the duration curve of windsurfing angle is given and the amplitude of the rolling motion is obtained by fast Fourier transform (Figs. 2 and 3).

According to the comprehensive analysis for the experimental data in Figs. 2 and 3, the sailboard rotates clockwise and anticlockwise around the horizontal position, and the amplitude of rolling angle decreases exponentially with time.

- In order to further prove the effectiveness of the proposed method, the curve of berthing force of windsurfing under the accompanying wave action of the wave group is given. The specific changes are shown in Fig. 3.

After analyzing the experimental data in Fig. 3, we can see that the ever-changing wave action leads to the ever-changing berthing force of windsurfing. The swaying motion of windsurfing consists of the simple harmonic oscillation around the balance position and the time-average drift along the wave propagation direction. The drift motion is generated by the second-order average drifting force. The heave motion and rolling motion of the sailboard show the form of simple harmonic oscillation basically, but the average dip angle of the roll motion is greater than zero.

- Running time/min.

In order to further prove the effectiveness of the proposed method, two traditional methods were selected as the comparison for simulation. The three methods need to be compared in running time. The specific experimental results are shown in Table 2.

Based on the above experimental results, we can see that the running time of the proposed method is significantly lower than traditional methods.

4. Conclusions

In traditional methods, the state of the water region is not considered comprehensively. Therefore, the research on the berthing force of windsurfing under the accompanying

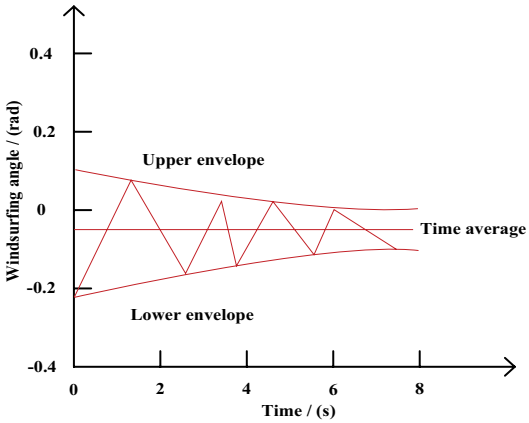

Fig. 2. Duration curve of windsurfing angle.

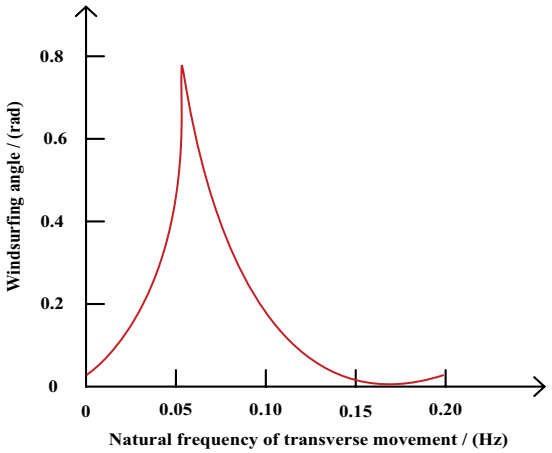

Fig. 3. Amplitude spectrum of windsurfing.

Table 1
Experimental wave elements of a physical model of windsurfing

Wave height H/(m)	Wave period T/(s)	Dimensionless water depth $d/(gT^2)$	Dimensionless wave height $H/(gT^2)$
0.06	1.0~2.0	0.015~0.066	0.15×10^{-2}~0.66×10^{-2}
0.08	1.0~2.0	0.015~0.066	0.21×10^{-2}~0.98×10^{-2}
0.10	1.0~2.0	0.015~0.066	0.27×10^{-2}~1.29×10^{-2}
0.12	1.2~2.2	0.015~0.043	0.33×10^{-2}~1.04×10^{-2}
0.14	1.2~2.2	0.015~0.043	0.40×10^{-2}~1.24×10^{-2}
0.16	1.2~2.2	0.015~0.043	0.46×10^{-2}~1.45×10^{-2}
0.18	1.2~2.2	0.015~0.045	0.48×10^{-2}~1.29×10^{-2}
0.20	1.2~2.2	0.015~0.045	0.50×10^{-2}~1.06×10^{-2}
0.22	1.2~2.2	0.015~0.045	0.52×10^{-2}~1.26×10^{-2}
0.24	1.4~2.4	0.015~0.045	0.54×10^{-2}~1.47×10^{-2}

Table 2
Change of operation time of the proposed method

Number of test samples	Operation time of [4]/(min)	Operation time of [5]/(min)	Operation time of the proposed method/(min)
100	15.96	18.96	12.01
200	17.89	20.17	13.36
300	19.63	22.69	14.25
400	21.74	–	15.20
500	23.20	24.78	16.23
600	25.78	26.85	17.45
700	27.41	28.66	18.63
800	29.63	30.47	19.58
900	31.74	32.58	20.11
1000	33.58	34.71	21.45
1100	35.96	36.85	22.58
1200	37.58	38.41	23.78
1300	39.41	40.25	24.69

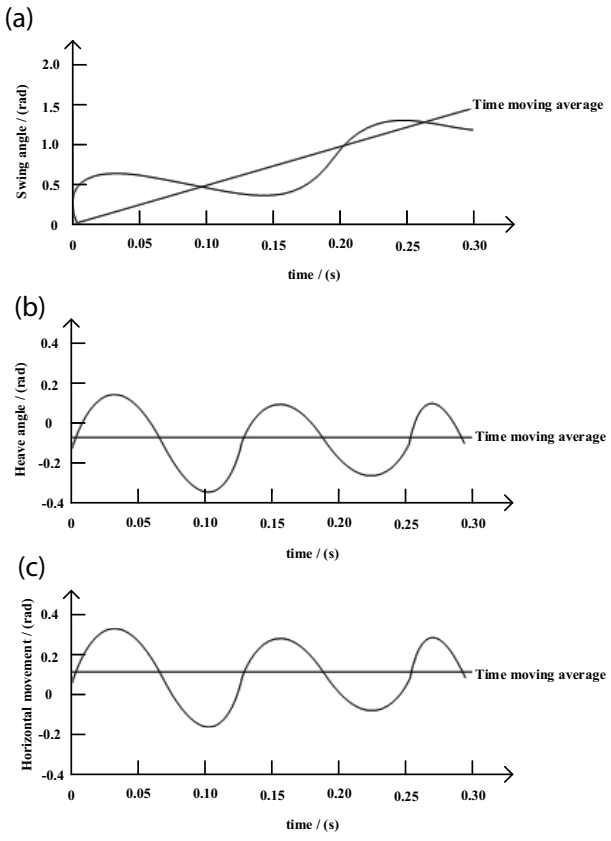

Fig. 4. Different berthing forces of windsurfing under accompanying wave action of wave group: (a) swaying motion, (b) heavy motion, and (c) rolling motion.

wave action of wave group was designed and proposed. Following conclusions can be drawn:

- The physical model test was designed. The image collection and data processing technology based on CCD was used to capture the movement of the floating structure and the change of wave surface. The problem that the traditional measurement method interferes with the flow field and affects the measurement accuracy was solved.
- In view of the defect of pressure field oscillation near the solid wall boundary in the SPH method, an improved model of calculating solid wall particle density was proposed, and the wave force on the structure of sailboard was obtained by the momentum equation.
- Through the simulation experiment data, the relationship between the accompanying wave action of wave group and berthing force of windsurfing was analyzed. The experimental data fully proved the effectiveness and practicability of the proposed method.

References

[1] X.W. Wang, J.M. Zhang, Elastoplastic dynamic response of saturated sandy seabed under random waves, Eng. Mech., 35 (2018) 26–30.
[2] X.Y. Kang, N.N. Liu, J. Li, T. Zhao, X.L. Xie, Dynamic response analysis of tunnels with parallel ground fissures under earthquake action, J. Eng. Geol., 26 (2018) 254–259.
[3] T.T. Sui, C. Zhang, Y.F. Gao, J.H. Zheng, Research on the liquefaction mechanism of the seabed around a single pile foundation under the action of waves, Ocean Eng., 36 (2018) 88–96.
[4] Z.Q. Huang, C. Li, Q.W. Ding, H.J. Chen, Dynamic response of wind wave load and analysis of mooring performance of floating submersible platform of floating wind turbine considering typhoon sea conditions, J. Power Eng., 37 (2017) 1015–1022.
[5] Q.W. Ding, C. Li, G.L. Zhou, Z. Ye, Comparison of dynamic response of land and sea wind turbines, J. Power Eng., 36 (2016) 65–73.
[6] M. Parvin, H. Chowdhury, A.K. Majumder, Water supply and sanitation facilities of some selected schools in Khagrachhari, Water Conserv. Manage., 3 (2019) 14–17.
[7] V.P. Govindan, P.M. Dhakate, A. Uniyal, Developmental human interface due to train collision of Asian Elephant (Elephas Maximus) in Western Circle Forest Division, Uttarakhand, India, Environ. Ecosyst. Sci., 3 (2019) 17–19.
[8] M. Kamal, R. Younas, M. Zaheer, M. Shahid, Treatment of municipal waste water through adsorption using different

waste biomass as activated carbon, J. Clean Was, 3 (2019) 21–27.
[9] L.J. Wu, Y.Z. Wang, Z. Xiao, Y. Li, Hydrodynamic response for flexible connectors of mobile offshore base at rough sea states, Pet. Explor. Dev., 43 (2016) 997–1004.
[10] B.E. Zhang, Y. Zheng, S.F. Fu, H.W. Liu, M.S. Zhao, C. Li, Experimental research on a new wave power generation conversion device, Chin. J. Electr. Eng., 39 (2019) 7263–7271.
[11] X.X. Huang, J.M. Yang, Y.R. Chen, Y. Jiang, Passive control of oscillating float wave power generation system based on PCHD model, Electr. Meas. Instrum., 56 (2018) 97–105.
[12] Y.T. Yang, R.C. Zhu, Y. Jiang, G.P. Liao, Three-dimensional non-reflective numerical wave pool and simulation of the interaction between waves and structures, J. Shanghai Jiaotong Univ. (Natural Edition), 52 (2018) 253–260.
[13] K. Xia, D.C. Wan, Numerical analysis of motion response characteristics of floating platforms near islands and reefs, Ocean Eng., 36 (2018) 10–17.
[14] Y.F. Deng, J.M. Yang, L.F. Xiao, X. Li, A review of studies on the generation of abnormal waves in wave pools, Ship Mech., 7 (2016) 967–970.
[15] D.C. Fritts, L. Wang, M.J. Taylor, P. Pautet, N.R. Criddle, B. Kaifler, S.D. Eckermann, B. Liley, Large-amplitude mountain waves in the mesosphere observed on 21 June 2014 during deepwave: 2. nonlinear dynamics, wave breaking, and instabilities, J. Geophys. Res., Atmospheres, 124 (2019) 17–18.
[16] C.W. Zhang, H. Wang, ARID control for suspended structure's swing vibration induced by multi–hazard source excitations, Vib. Shock, 38 (2019) 25–32.
[17] Q. Yang, H.J. Liu, Dynamic response of multilayered silty seabeds under wave–current action in the yellow river estuary, Int. J. Geomech., 18 (2018) 04018031.1–04018031.11.
[18] S.L. Zhang, Structural strength analysis of superyachts with superstructures of different materials in waves, J. Wuhan Univ. Technol. (Transport Science and Engineering Edition), 40 (2016) 97–100.
[19] Y.L. He, Y.X. Ma, X.Z. Ma, G.H. Dong, Experimental analysis of non-linear evolution of deep-water independent wave group, J. Harbin Eng. Univ., 40 (2019) 1839–1845.
[20] Y. Huang, Research on hydrodynamic characteristics of wave energy power plant, J. Phys.: Conf. Ser., 1634 (2020) 012144 (7 p).
[21] J.H. Chow, E.Y.K. Ng, N. Srikanth, Numerical study of the dynamic response of a wind turbine on a tension leg platform with a coupled partitioned six degree–of–freedom rigid body motion solver, Ocean Eng., 172 (2019) 575–582.
[22] M. Yue, Q. Liu, C. Li, Q. Ding, H. Zhu, Effects of heave plate on dynamic response of floating wind turbine Spar platform under the coupling effect of wind and wave, Ocean Eng., 201 (2020) 107103.
[23] Z. Liu, L. Li, D. Lv, N. Pan, Novel source recovery method of underdetermined time–frequency overlapped signals based on submatrix transformation and multi–source point compensation, IEEE Access, 7 (2019) 29610–29622.
[24] L. Li, H.Y. Jiao, X.L. Du, P.X. Shi, Fully fluid–solid coupling dynamic model for seismic response of underground structures in saturated soils, Earthquake Eng. Eng. Vib., 19 (2020) 4–15.
[25] X.Y. Liang, X.W. Wang, Y. Wang, Dynamic response of soft-core sandwich beams subjected to moving points, J. Nanjing Univ. Aeronaut. Astronaut., 48 (2016) 544–550.
[26] A.D.G. Mahunon, Investigation of the fatigue behaviour of a ballastless slab track–bridge structural system under train load, Appl. Sci., 9 (2019) 3625.
[27] C.B. Xiong, Y. Guo, Dynamic response analysis of saturated porous foundation considering thermal-hydro-mechanical coupling effect, Appl. Math. Mech., 39 (2018) 689–699.
[28] Z.L. Zhang, S.R. Wu, T. Wang, Effect of seismic wave amplitude on the dynamic response of loess-mudstone slopes, Rock Soil Mech., 39 (2018) 93–96.
[29] F.R. Carrillo Pedroza, M.D.J. Soria Aguilar, M.A. Sanchez Castillo, A. Martinez Luevanos, N.G. Picazo Rodriguez, Adsorption of chromium from steel plating wastewater using blast furnace dust, Revista Internacional De Contaminacion Ambiental, 33 (2017) 591–603.
[30] M.M. Morones Esquivel, J.C. Pantoja Espinoza, J.B. Proal Najera, I. Chairez Hernandez, J.N. Gurrola Reyes, M. Avila Santos, Use of a plate reactor (TiO_2/glass) for the degradation of 2,5-diclorofenol by solar photocatalysis, Revista Internacional De Contaminacion Ambiental, 33 (2017) 605–616.
[31] Q. Quan, H. Zou, X.F. Huang, J.C. Lei, Research on water temperature prediction based on improved support vector regression, Neural Comput. Appl., (2020).